PCCP

PAPER

View Article Online
View Journal | View Issue

Cite this: *Phys. Chem. Chem. Phys.*, 2014, **16**, 21340

The impact of ionic liquid fluorinated moieties on their thermophysical properties and aqueous phase behaviour†

Catarina M. S. S. Neves,[a] Kiki A. Kurnia,[a] Karina Shimizu,*[b] Isabel M. Marrucho,[c] Luís Paulo N. Rebelo,[c] João A. P. Coutinho,[a] Mara G. Freire*[a] and José N. Canongia Lopes[bc]

Received 8th May 2014,
Accepted 22nd August 2014

DOI: 10.1039/c4cp02008a

www.rsc.org/pccp

In this work, we demonstrate that the presence of fluorinated alkyl chains in Ionic Liquids (ILs) is highly relevant in terms of their thermophysical properties and aqueous phase behaviour. We have measured and compared the density and viscosity of pure 1-ethyl-3-methylimidazolium tris(pentafluoroethyl)trifluorophosphate, $[C_2C_1im][FAP]$, with that of pure 1-ethyl-3-methylimidazolium hexafluorophosphate, $[C_2C_1im][PF_6]$, at atmospheric pressure and in the (288.15 to 363.15) K temperature range. The results show that the density of $[C_2C_1im][PF_6]$ is lower than that of $[C_2C_1im][FAP]$, while the viscosity data reveal the opposite trend. The fluid phase behaviour of aqueous solutions of the two ILs was also evaluated under the same conditions and it was found that the mutual solubilities of $[C_2C_1im][FAP]$ and water are substantially lower than those verified with $[C_2C_1im][PF_6]$. The experimental data were lastly interpreted at a molecular level using Molecular Dynamics (MD) simulation results revealing that the interactions between the IL ions and the water molecules are mainly achieved *via* the six fluorine atoms of $[PF_6]^-$ and the three analogues in $[FAP]^-$. The loss of three interaction centres when replacing $[PF_6]^-$ by $[FAP]^-$, coupled with the bulkiness and relative inertness of the three perfluoroethyl groups, reduces its mutual solubility with water and also contributes to a lower viscosity displayed by the pure [FAP]-based IL as compared to that of the $[PF_6]$-based compound.

Introduction

Ionic liquids (ILs) have appeared, in the past few years, as potential alternatives or complements to the over six hundred common solvents used in industry. This class of compounds is usually composed of large organic cations and organic or inorganic anions, which allow them to remain liquid at or near room temperature and at atmospheric pressure. Most of these fluids have a unique combination of properties, namely their high thermal and chemical stabilities, large range of temperatures in which they are liquid, high ionic conductivity, large electrochemical window, negligible vapour pressure, non-flammability and a high solvating capacity for organic, inorganic and organometallic compounds. Some of these properties led to a large amount of research studies through their exploitation as alternative and "greener" solvents.[1,2] In addition, the huge number of possible combinations between cations and anions (*circa* 10^6 of different ILs)[3] allows their tuning, meaning that they can be designed for a particular application or to show a specific set of intrinsic properties, and thus they are also often described as "designer solvents".[3] In the environmental field and concerning the atmospheric pollution, appropriate ILs display negligible vapour pressures and can substitute the typically employed volatile organic compounds (VOCs). However, their non-significant vapour pressures are not enough to assure that these compounds are in fact "green". Even hydrophobic ILs, defined as those that form two phases with water under atmospheric conditions, exhibit a measurable solubility in water,[4–13] and therefore can lead to water contamination. Furthermore, the presence of water in ILs affects significantly their physical properties.[12,14,15] It is therefore of vital importance to characterize the mutual solubilities between different ILs and water aiming at addressing their environmental impact and possible deviations in their thermophysical properties.

In this work, a systematic study was conducted on the densities and viscosities of pure ILs and their mutual solubilities with water

[a] *Departamento de Química, CICECO, Universidade de Aveiro, 3810-193 Aveiro, Portugal. E-mail: maragfreire@ua.pt*
[b] *Centro de Química Estrutural, Instituto Superior Técnico, Universidade de Lisboa, 1049-001 Lisboa, Portugal. E-mail: karina.shimizu@ist.utl.pt*
[c] *Instituto de Tecnologia Química e Biológica, ITQB2, Universidade Nova de Lisboa, Av. República, Apartado 127, 2780-901 Oeiras, Portugal. Web: www.itqb.unl.pt*

† Electronic supplementary information (ESI) available: Comparison of the experimental data obtained here with those reported in the literature. See DOI: 10.1039/c4cp02008a

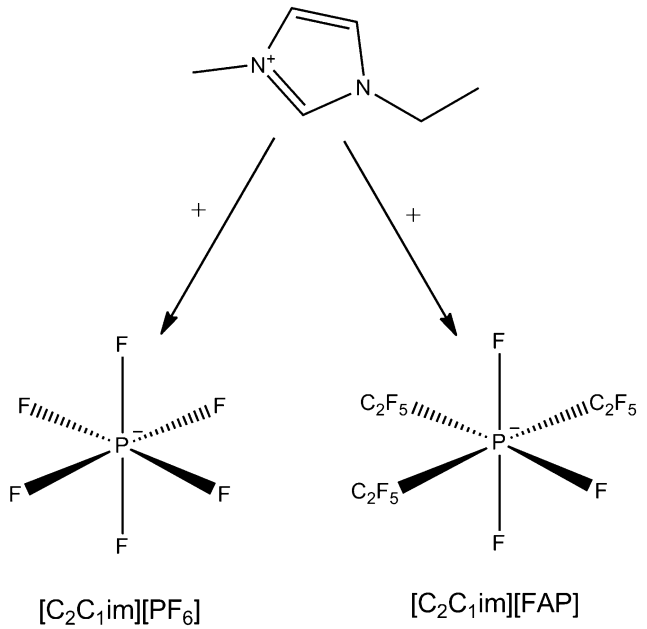

Scheme 1 Structures of the ions that compose the ILs studied in this work.

in a wide temperature range. These studies have allowed us to understand, in a deeper manner, the influence of the fluorinated alkyl chains in the anion, by comparing the hexafluorophosphate ($[PF_6]^-$) and tris(pentafluoroethyl)trifluorophosphate ($[FAP]^-$) anions, both combined with the 1-ethyl-3-methylimidazolium ($[C_2C_1im]^+$) cation. Scheme 1 depicts the structures of the ions that compose the investigated ILs. The *cis* and *trans* positions of the C_2F_5-groups and the fluorine atoms in the structure of the $[FAP]^-$ anion of the IL studied in this work were determined by us by ^{19}F NMR (*cf.* Fig. S1 in ESI†).

Molecular Dynamics (MD) simulation data were further used to interpret the experimental results at a molecular level.

Results and discussion

The main point of the present work is the comparison of the distinct behaviour of two ILs that are somewhat related (same cation and substitution in the anion of three fluorine atoms by three fluorinated ethyl groups), namely $[C_2C_1im][PF_6]$ and $[C_2C_1im][FAP]$, aiming for a deeper understanding of the effect of substituting fluorine atoms by fluorinated alkyl chains through the thermophysical properties and aqueous phase behaviour.

Melting temperature

The melting temperature of the dried $[C_2C_1im][PF_6]$, solid at room temperature, was determined by DSC. Only one phase transition was observed in the temperature range evaluated. The melting temperature obtained was 333.83 K that is in good agreement with the literature.[10] For the same sample, the enthalpy change at the corresponding melting temperature, from the crystal to the isotropic liquid phase transition, is 17.1 kJ mol^{-1}. The melting temperature reported for $[C_2C_1im][FAP]$ is 236.15 K,[16] thus significantly lower than that observed for $[C_2C_1im][PF_6]$. This is a result of the larger [FAP] anion which contributes for a reduction of the structural (crystalline) organization of the ions, therefore leading to lower melting temperatures.

Density

The experimental density data for pure and dried ILs are presented in Table S1 in the ESI.† For $[C_2C_1im][FAP]$ the temperature interval attempted ranges between (278.15 and 363.15) K. Due to the higher melting temperature of $[C_2C_1im][PF_6]$, densities and viscosities were only determined at temperatures above 338.15 K. This work presents, for the first time, experimental density data for $[C_2C_1im][PF_6]$. Fig. S2 in ESI† depicts the relative deviations between the experimental density data obtained here and in the literature for $[C_2C_1im][FAP]$.[17–20] The maximum relative deviation between our data and those previously published[17–20] is below 1%.

The experimental density data for the studied ILs are shown in Fig. 1. The density of the hexafluorophosphate-based IL is substantially lower than that displayed by $[C_2C_1im][FAP]$ in the temperature range investigated. As far as the volumetric properties are concerned, at 343.15 K, the differences can be mostly ascribed to a higher percentage of heavier atoms in the latter IL. Conversely, the large difference in the corresponding molar volumes (at 343.15 K, 178.6 cm^3 mol^{-1} for $[C_2C_1im][PF_6]$ and 338.6 cm^3 mol^{-1} for $[C_2C_1im][FAP]$) can be attributed to the much higher molar mass of $[C_2C_1im][FAP]$ relative to that of $[C_2C_1im][PF_6]$.

The isobaric thermal expansion coefficient (α_p), which considers the volumetric changes with temperature, was calculated from the fitting of the experimental data using eqn (1),

$$\alpha_p = -\left(\frac{\partial \ln \rho}{\partial T}\right)_p \quad (1)$$

where ρ is the density in kg m^{-3}, T is the temperature in K and p is the pressure in MPa.

The thermal expansion coefficients are very close and vary between (5.94 and 7.84) $\times$ 10^{-4} K^{-1} for both ILs. $[C_2C_1im][FAP]$ exhibits a lower thermal expansion coefficient than $[C_2C_1im][PF_6]$. These values are considerably lower than those observed with

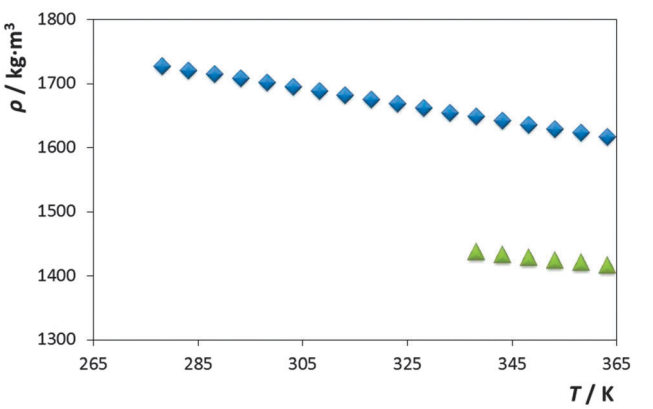

Fig. 1 Experimental density as a function of temperature and at 0.1 MPa for the ILs: $[C_2C_1im][FAP]$ (blue ◆); $[C_2C_1im][PF_6]$ (green ▲).

molecular organic solvents and higher than those of classical molten salts.[21]

Viscosity

As for the density measurements, the viscosity data were determined in the temperature range from (278.15 to 363.15) K for the $[C_2C_1im][FAP]$ and from (338.13 to 363.15) K for the $[C_2C_1im][PF_6]$. The experimental results are presented in Table S1 in the ESI† and in Fig. 2. Fig. S3 in ESI† depicts the relative deviations between our work and literature data for $[C_2C_1im][FAP]$.[17,19] The maximum relative deviation found was 4.3%. Taking into consideration that the viscosity of ILs is highly sensitive to the water content and to the purity level of the sample, it can be stated that our data are in close agreement with the literature.[17,19]

Since viscosity is mainly dependent on intermolecular interactions (H-bonding, dispersive and Coulombic interactions), an increase in temperature will substantially decrease the intensity of H-bonding interactions and, therefore, the viscosity decreases with the increase in temperature. In general, and at all the temperatures studied, $[C_2C_1im][PF_6]$ is more viscous than $[C_2C_1im][FAP]$, and follows the opposite behaviour to that observed in density results. The charge density in the two ILs and its distribution is quite distinct,[22,23] with an important impact on their viscosity. Moreover, the substitution of 3 F atoms by three perfluoroethyl groups in [FAP]-based ILs leads to a lower viscosity also resulting from weaker cation–anion interactions.

IL + water mutual solubilities

The measured solubility data and the respective standard deviations are presented in Table S2 in ESI.† The representation of the respective phase diagrams is depicted in Fig. 3.

The comparison of the results obtained here with those already reported in the literature[6,10] is depicted in Fig. S4 in ESI.† For the aqueous system with $[C_2C_1im][FAP]$, the values obtained in this work are in close agreement with those reported by Domańska *et al.*[6] Nevertheless, the major differences between authors are observed in the IL-rich phase, and at higher temperatures. In this work, the water content in the IL-rich phase was measured by Karl–Fischer (KF) titration, whereas the values reported in the literature were obtained by a dynamic (synthetic) method.[6]

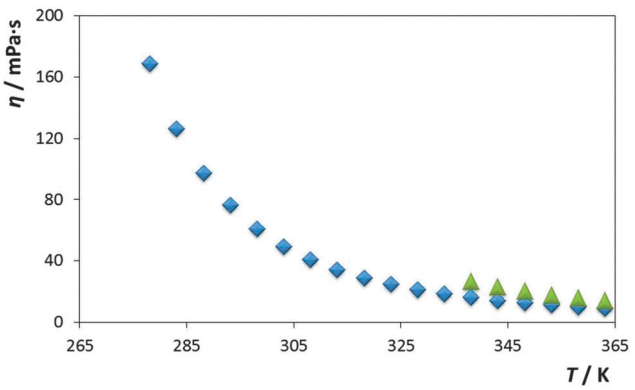

Fig. 2 Experimental viscosity as a function of temperature and at 0.1 MPa for the ILs: $[C_2C_1im][FAP]$ (blue ◆); $[C_2C_1im][PF_6]$ (green ▲).

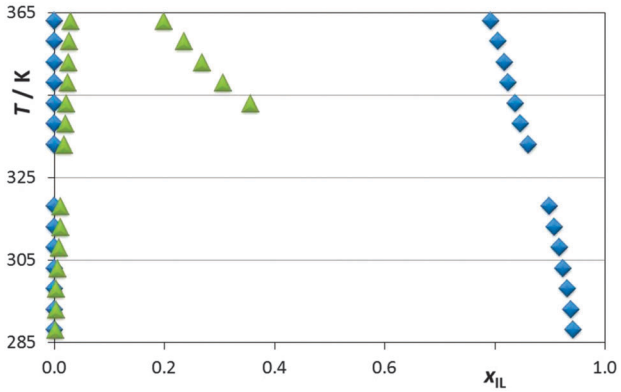

Fig. 3 Liquid–liquid phase diagram for the binary system composed of water and ILs: $[C_2C_1im][FAP]$ (blue ◆); $[C_2C_1im][PF_6]$ (green ▲).

On the other hand, the liquid–liquid equilibrium results for $[C_2C_1im][PF_6]$ obtained in this work and those reported in the literature[10] display significant differences. This should be mainly related to the purity of the IL used as well as to the different experimental techniques employed. The solubility values of the IL in water reported in the literature were obtained by KF titration.[10] However, it should be stressed that this method is not the most accurate to determine such large amounts of water at a water-rich phase.

Regarding our results, for both ILs, the mutual solubilities increase with increasing temperature, a fact that suggests an upper critical solution temperature behaviour. The mole fraction solubility of $[C_2C_1im][FAP]$ in water is in the order of $\approx 10^{-5}$, while with $[C_2C_1im][PF_6]$, the solubility in water is in the order of $\approx 10^{-3}$. Instead, the water mole fraction solubility in $[C_2C_1im][FAP]$ is around 10^{-2}, and for $[C_2C_1im][PF_6]$ it is in the order of $\approx 10^{-1}$, indicating that both ILs are highly "hygroscopic", as previously shown for other hydrophobic ILs.[5,12,24,25] Thus, while the water-rich phase can be considered as an almost pure phase with the IL at infinite dilution, the IL-rich phase exhibits a significant content of water. Overall, the mutual solubilities between water and ILs are much lower for the IL composed of the longer aliphatic fluorinated tails. This trend is the opposite of that observed in the liquid–liquid equilibrium of binary mixtures involving fluorinated ILs and perfluorocarbons.[26] Although an upper critical solution temperature is also observed, an increase in the fluorinated chain length of the IL anion increases the perfluorocarbon solubility.[26]

The extremely skewed phase diagram presented in Fig. 3 can be re-plotted taking into account: (i) the large differences between the molar volume (charge density) of the two ILs; and (ii) between those and the molar volume of water. The phase diagrams given in Fig. 4a and b (as a function of the weight and volume fractions occupied by the IL component, respectively) yield much more symmetrical diagrams that emphasize the much lower mutual solubilities of $[C_2C_1im][FAP]$ and water relative to those of $[C_2C_1im][PF_6]$, both for the water-rich and IL-rich compositions. The diagrams of Fig. 3 and 4 alert for the fact that any comparison between these systems must take into account the intrinsic differences in molar volume of the different components.

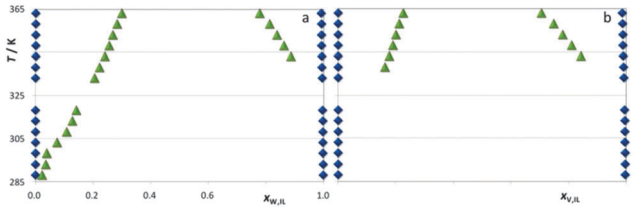

Fig. 4 Liquid–liquid (T–x) phase diagrams as a function of (a) weight, $x_{W,IL}$ (b) and volume fraction, $x_{V,IL}$ for the binary system composed of water and $[C_2C_1im][FAP]$ (blue ◆) and $[C_2C_1im][PF_6]$ (green ▲). For $[C_2C_1im][PF_6]$ the $x_{V,IL}$ was only calculated for temperatures above 338.15 K due to its higher melting point and lack of density data at lower temperatures.

Molecular dynamics simulations

The phase behaviour of the two ILs, namely in binary mixtures with water, were determined by the nature, distribution and density of the interaction centres of the ions that are capable of strong interactions with water molecules (the aromatic hydrogen atoms in the imidazolium cation and the fluorine atoms directly connected to the phosphorus atom of the anion).

Several Molecular Dynamics (MD) simulations were performed in order to explore the relation between the phase behaviour in the binary mixtures and the underlying interactions at a molecular level.

Fig. 5 shows the radial distribution functions between the charged parts of the anions and cations in the pure ILs (continuous lines) and in the water-rich solutions (dotted lines). The grey, red and blue functions are a sort of fingerprint of an IL: due to the ionic character of the liquid, any given ion will be surrounded by alternating shells of counter-ions and same-charge-ions. This can be appreciated in the snapshots of Fig. 5c and d where the polar network of the ILs can be noticed as blue areas (cations) surrounded by red areas (anions) in a three-dimensional and continuous arrangement. Fig. 5a and b show the same opposition-of-phase character of the anion–cation (grey) *versus* anion–anion (red) or cation–cation (blue) correlations. This periodicity and its characteristic wavelength is rather different in the two pure ILs and is a measure of the morphology of the polar network in each case: both are continuous but more stretched and string-like in $[C_2C_1im][FAP]$ than in the case of $[C_2C_1im][PF_6]$ (the former has to accommodate the bulky – C_2F_5 moieties of its anion – depicted as green space-filled atoms in Fig. 5c – whereas the latter does not have to). Interestingly, the elongation of the wavelength of the polar network (from shell-to-shell distances of around 0.32 nm in $[C_2C_1im][PF_6]$ to around 0.40 nm in $[C_2C_1im][FAP]$) corresponds approximately to the ratio of the molar volumes ($(0.32/0.39)^3 \approx 0.54 \approx 178.6/338.6$) of the two pure ILs. In other words, both ILs are characterized by a polar network of the charged parts of their ions but, whereas such network occupies most of the available volume in $[C_2C_1im][PF_6]$, it is more stretched and has to encompass rather large non-polar moieties in the case of $[C_2C_1im][FAP]$.

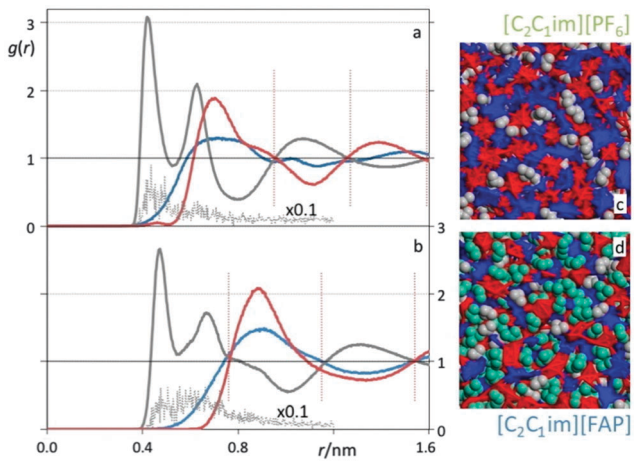

Fig. 5 Selected radial distribution functions (RDFs), $g(r)$, as a function of distance, r, for the (a) $[C_2C_1im][PF_6]$ and (b) $[C_2C_1im][FAP]$ ILs. Grey lines: RDFs between the imidazolium ring centroid of the cation, im, and the phosphorus atom of the anion, P; blue lines: im–im RDFs; red lines: P–P RDFs. The dotted grey lines correspond to im–P RDFs (with its intensities divided by 10) obtained at infinite dilution in water. The dotted vertical lines show the periodicity of the alternating shells of ions and counter-ions surrounding a given ion. The MD simulation snapshots (c, d) are color-coded to reflect the presence of the charged parts of the cations (blue), the charged parts of the anions (red), the alkyl side chains of the cation (grey), and, in the case of $[C_2C_1im][FAP]$, the perfluoroalkyl chains of the anion (green).

When the IL ions are diluted in water (by placing just one pair of ions in the midst of hundreds of water molecules in the MD simulations), the corresponding anion–cation RDFs (grey dotted lines in Fig. 5a and b) show intense peaks at approximately the same positions of the pure compounds RDFs. The intensity of the peaks (the RDFs have been divided by a factor of ten in order to fit a single graph) is a consequence of the normalization of all RDFs. Whenever the two ions contained in the simulation box interact with each other for longer periods, or more frequently than the values preordained by pure random encounters, such correlations will contribute disproportionately to the first peak of the RDFs. If more ions were to be found in the simulation box, one would expect that these would start to form small ionic clusters in the solution, *i.e.*, a preliminary phase separation process. Nevertheless, it should be stressed that we did not perform simulations under such conditions since the results do not correspond to single-phase conditions.

Fig. 6 shows the hydrogen–oxygen RDFs in almost pure water (Fig. 6a) and of water diluted in the midst of the ILs (Fig. 6b). Fig. 6a shows RDFs that are almost indistinguishable between them and almost identical to that of pure water. The first peak corresponds to the hydrogen bond between two water molecules, and the second to the correlation between the oxygen of one of the molecules and the second hydrogen (not H-bonded to that oxygen) of the second water molecule. Unlike the RDFs of the ILs, the RDF of water converges rapidly to unity and does not show any medium-range periodicity. However, the two peaks attest the strength and directionality of the underlying H-bond interactions. The structure of liquid water is a highly distorted random network of hydrogen bonded species.

When water molecules are diluted in the highly organized IL medium (Fig. 6b) it is observed that water–water hydrogen bonding still occurs (the corresponding peaks are found at

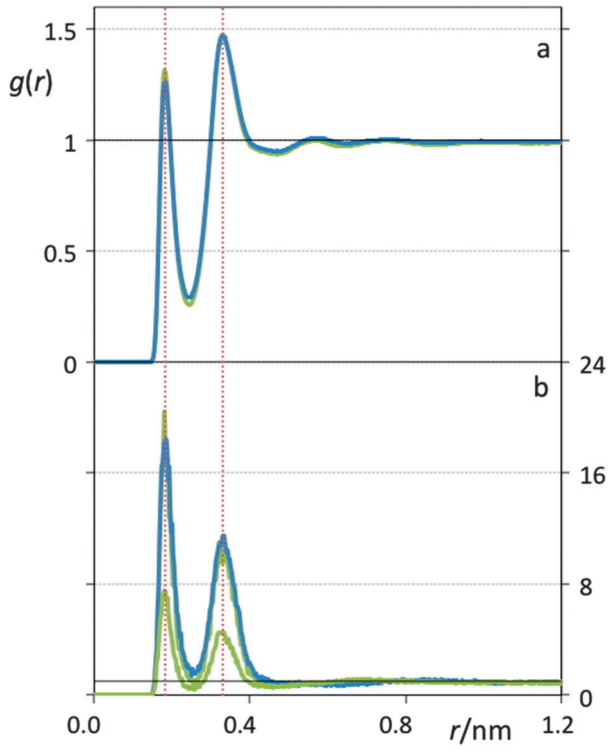

Fig. 6 Water O–H radial distribution functions (RDFs), $g(r)$, as a function of distance, r. (a) Water-rich $[C_2C_1im][PF_6]$ (green line) and $[C_2C_1im][FAP]$ (blue line) solutions containing one IL ion pair per 600 water molecules. The two lines are nearly superimposed. (b) IL-rich aqueous solutions containing 200 $[C_2C_1im][FAP]$ ion pairs and 20 water molecules (blue line), or 200 $[C_2C_1im][PF_6]$ ion pairs and 20 or 11 water molecules (green lines). One of the green lines (corresponding to the solution with 11 water molecules) is almost superimposed with the blue line.

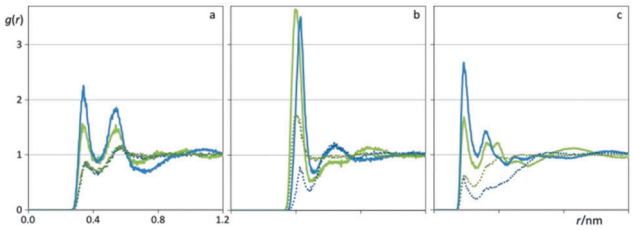

Fig. 7 Water–IL radial distribution functions (RDFs), $g(r)$, as a function of distance, r. The four lines in each panel correspond to $[C_2C_1im][PF_6]$ IL-rich solutions (solid green), $[C_2C_1im][FAP]$ IL-rich solutions (solid blue), $[C_2C_1im][PF_6]$ water-rich solutions (dotted green) and $[C_2C_1im][FAP]$ water-rich solutions (dotted blue). (a) RDFs between the CR atom (see text) of the cation and the oxygen atom of water; (b) RDFs between the phosphorus atom of the anions and the oxygen atom of water; (c) RDFs between three fluorine atoms (see text) of the anions and the hydrogen atom of water.

the same distances observed for pure water) and much more frequently than the values expected based on purely random distributions of water in the ILs. This situation is consistent with possible phase separation at higher water concentrations. Fig. 6b also shows another relevant fact: if the water–water RDFs are compared at the same mole concentration of water (20 water molecules in 200 IL ion pairs), the intensity of the peaks is quite different and larger for $[C_2C_1im][FAP]$. This pattern does not mean that the water–water interactions are more intense in the former IL than in the latter, just that since the numerical density (number of water molecules *per* volume of solution) is smaller in the $[C_2C_1im][FAP]$ solution than it is in $[C_2C_1im][PF_6]$, the normalization of the RDFs implies that the same number of hydrogen bond contacts in the $[C_2C_1im][FAP]$ aqueous medium produces a more intense peak. This can be proven if one makes the comparison at approximately the same numerical density of water molecules—keeping the 20 water molecules in 200 IL ion pairs for the $[C_2C_1im][FAP]$ and reducing that number to 11 water molecules in 200 IL ion pairs for $[C_2C_1im][PF_6]$. In that case, the two RDFs are almost superimposed, implying that if the density of water molecules in the IL is the same, the amount and intensity of the hydrogen bonds between them is also similar. On one hand, we have to be particularly aware of the implications caused by the large difference in the molar volume of the two ILs, and, on the other hand, the large differences in mutual solubilities of water and the two ILs after the volume effects are discounted must originate in cross interaction (water–IL) differences between the components and not from any significant shift in the self-interactions (water–water or IL–IL).

The correlations between the atoms involved in the cross interactions between the water molecules and the ions that compose the ILs are depicted in Fig. 7. Panel 7a depicts the correlation between the oxygen atom of water and the carbon atom of the imidazolium ring between the two nitrogen atoms (CR) for the IL-rich (solid lines) and water-rich (dotted lines) solutions. Again, the intensity of the first peaks of the solid lines seem to indicate that the cation–water interactions in $[C_2C_1im][FAP]$ (blue solid line) are stronger than those in $[C_2C_1im][PF_6]$ (green solid line). However, this is again an effect caused by the different numerical density of water when diluted in the two ILs. Panel 7b shows the anion–water interactions by depicting the RDFs between the oxygen atom of water and the phosphorus atom of the anions. The intensity of the two solid peaks (IL-rich solutions) is now very similar and much more intense than the corresponding cation–water interactions; yet, the water–anion interactions in $[C_2C_1im][FAP]$ are weaker than in the corresponding $[C_2C_1im][PF_6]$ solutions if numerical density arguments are invoked. This is further corroborated by the water-rich RDF data. At approximately the same numerical density, the anion–water interactions in the $[C_2C_1im][PF_6]$ solutions are more intense (green dotted peak) than the corresponding interactions in the $[C_2C_1im][FAP]$ solutions (blue dotted peak). This constitutes the greater difference between the two solutions: anion–water interactions (that are the dominant cross interactions in these systems, *cf.* panels a and b of Fig. 7) with $[FAP]^-$ are weaker than those with $[PF_6]^-$, simply because one has more interaction centres in the former anion (six electronegative fluorine atoms connected to the phosphorus atom) than in the latter. This behaviour can be analysed in Fig. 7c that shows the RDFs corresponding to the correlation between the hydrogen atoms of the water molecules and the fluorine atoms of the anions connected to the phosphorus atom.

In order to avoid further numerical density problems, we have decided to compare the three fluorine atoms directly attached to the phosphorus atom in $[FAP]^-$ to three of the six fluorine atoms of $[PF_6]^-$. The results in Fig. 7 show that the intensities of the H–F interactions are very similar for both ILs if their different molar volumes are taken into account. The first peaks of the dotted lines in the water-rich solutions have almost identical intensities, whereas the first peaks of the solid lines in the IL-rich solutions show larger intensities for the $[C_2C_1im][FAP]$ solutions, due to the normalization effect already discussed for the water–water and cation–water interactions. In other words, individual H(water)–F(anion) interactions are similar in both types of solutions, but the overall water–anion interactions are more intense in $[C_2C_1im][PF_6]$, simply because there are six instead of three available electronegative fluorine atoms.

In respect to the other fluorine atoms in the $[FAP]^-$ ion (those attached to the perfluoroethyl groups), Fig. 8a shows that the correlations between those groups in pure $[C_2C_1im][FAP]$ or in $[C_2C_1im][FAP]$-rich solutions are not very intense. In fact, they are approximately as intense as those between the terminal methyl groups of the ethyl side chains of the $[C_2C_1im]^+$ cation.[27] These perfluoroethyl groups, like their hydrogenated counterparts in the cation, form small non-polar aggregates in the midst of the polar network, confirming the already discussed "stretching" of the polar network and the much large molar volume of $[C_2C_1im][FAP]$. Moreover, Fig. 8b shows that the interactions between the fluorine atoms of the perfluoroethyl chains and the hydrogen atoms of the water molecules are quite weak. Unlike the H–F RDFs of Fig. 7c, there are no peaks at distances (*ca.* 0.2 nm) compatible with hydrogen-bonding. The peaks shown in Fig. 8b, at distances above 0.4 nm, simply correspond to correlations between the hydrogen atoms of water that form hydrogen bonds with the $-PF_3$ fluorine atoms and the neighbouring fluorine atoms of the $-CF_2-$ and $-CF_3$ groups.

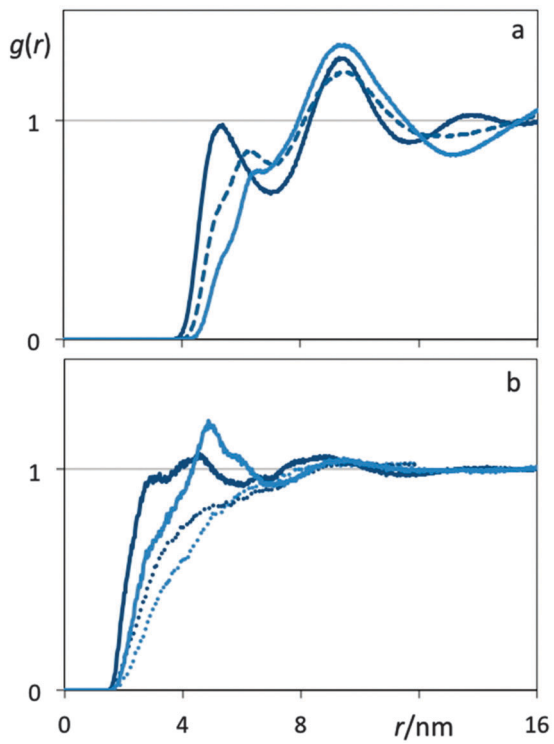

Fig. 8 (a) Perfluoroethyl–perfluoroethyl radial distribution functions (RDFs), $g(r)$, as a function of distance, r, in $[C_2C_1im][FAP]$ IL-rich solutions. The dark blue line corresponds to correlations between the terminal carbon atoms of the perfluoroethyl groups; the light blue one to correlations between the carbons attached to the phosphorus atom; and the dashed line to correlations between the two types of carbon. (b) Water–perfluorethyl radial distribution functions (RDFs), $g(r)$, as a function of distance, r, in $[C_2C_1im][FAP]$ IL-rich solutions (solid lines) and water-rich solutions (dotted lines). The dark blue line corresponds to correlations between the hydrogen atom of water and the $-CF_3$ fluorine atoms of the perfluoroethyl groups; the light blue one to correlations between the hydrogen atom of water and the $-CF_2-$ fluorine atoms of the perfluoroethyl groups.

In summary, the mutual solubilities of $[C_2C_1im][FAP]$ or $[C_2C_1im][PF_6]$ with water can be rationalized taking into account the following facts: (i) the asymmetrical nature of the immiscibility windows (Fig. 3) can be "corrected" if one takes into account the different molar volumes of the two ILs (Fig. 4); (ii) both pure components are characterized by strong intermolecular interactions. The investigated ILs are electrostatic in nature and lead to a mesoscopic ordered polar network, interspersed with non-polar domains that are much larger in $[C_2C_1im][FAP]$ than in $[C_2C_1im][PF_6]$ (*cf.* Fig. 5a and b). Indeed, the formation of three nanosegregated domains (polar, nonpolar, and fluorous) has been already observed in other fluorinated ILs.[28] In the case of water, the liquid phase is characterized by a disordered but tightly connected hydrogen-bonded three-dimensional network (Fig. 6). In order to mix these two types of components, the cross interactions in the mixture must compensate the partial loss of the strong interactions within the pure components; (iii) both systems exhibit immiscibility windows because in neither example the cross interactions are strong enough to disrupt completely the established networks. The immiscibility window of $[C_2C_1im][FAP]$ is much larger than that of $[C_2C_1im][PF_6]$ due to the fact that the most important cross interactions (those between the anion and water, namely the interactions between the fluorine atoms attached to the phosphorus atom and the hydrogen atoms of water) are overall weaker in the former than in the latter IL (Fig. 7b). This is a direct result of the six fluorine interaction centres in $[PF_6]^-$ and only three in $[FAP]^-$ (compare Fig. 8b with Fig. 7b).

Finally, the direct estimation of the viscosity of ILs using MD is a relatively difficult procedure due to the fact that most of the force-fields commonly used (including CL&P[22,23,29]) are non-polarizable and thus yield diffusion coefficients that are sometimes almost one order of magnitude lower than the experimental results. The high viscosity of most ILs also implies unreasonably long simulation runs. Nevertheless, it is possible to infer some conclusions about the viscosity difference between the two neat ILs by reconciling the trends of the self-diffusion coefficients of the two ions with all that was previously discussed concerning their distinct nano-structuration, molar volume and charge density distribution. Nevertheless, it should

be remarked that some literature reports already pointed out the correlation between the ionicity of ILs and their physicochemical properties.[30–33] At 338 K, the 8 ns-long MD runs on the pure systems have yielded self-diffusion coefficients of 15 and 5 $m^2\ Ts^{-1}$ for the diffusion of the $[C_2C_1im]^+$ cations in $[C_2C_1im][FAP]$ and $[C_2C_1im][PF_6]$, respectively, and 8 and 3 $m^2\ Ts^{-1}$ for the diffusion of the $[FAP]^-$ and $[PF_6]^-$ anions in $[C_2C_1im][FAP]$ and $[C_2C_1im][PF_6]$, respectively. Even if the uncertainty associated with these values is high and the comparisons are performed on a semi-quantitative basis, the trends—the diffusion coefficients of the ions are three times higher in the [FAP]-based than in the $[PF_6]$-based IL in spite of the fact that the anions of the former IL are much bulkier—suggest that the loss of strong interaction centres when one substitutes the $[PF_6]^-$ ion by the $[FAP]^-$ ion does indeed lead to a less coordinated and more flexible polar network. Albeit the presence of bulkier groups in $[FAP]^-$, this leads to higher ionic mobilities in the [FAP]-based IL than in its $[PF_6]$-based counterpart.

Experimental

Materials

1-Ethyl-3-methylimidazolium tris(pentafluoroethyl)trifluorophosphate, $[C_2C_1im][FAP]$, and 1-ethyl-3-methylimidazolium hexafluorophosphate, $[C_2C_1im][PF_6]$ were supplied by Merck and Iolitec, respectively, with purity levels higher than 98 wt%. These ILs were further purified (to reduce the content of water and other volatile components), by drying individual samples at *circa* 353 K for at least 48 h, and under constant stirring and moderate vacuum conditions ($\approx$0.1 Pa). After this procedure, ^1H, ^{13}C, ^{31}P and ^{19}F NMR analyses confirmed the purity of the IL samples.

Double-distilled water (passed through a reverse osmosis system and further treated using a MilliQ plus 185 water purification apparatus) was used in the preparation of all (IL + water) binary mixtures. Purity analyses revealed resistivity values of 18.2 MΩ cm and a TOC (Total Organic Carbon content) smaller than 5 $\mu g\ dm^{-3}$. The analyte used for the coulometric Karl–Fischer (KF) titration was Hydranal® – Coulomat AG from Riedel-de Haën. Before the experimental measurements, the water content of the pure ILs, measured by KF, was below 200 ppm.

Experimental procedure

Differential scanning calorimetry measurements. The IL $[C_2C_1im][PF_6]$ is not liquid at room temperature and the respective melting temperature was determined using a Diamond Differential Scanning Calorimetry (DSC) PerkinElmer equipment. The sample was tightly sealed in an aluminium pan. The temperature scans were of 0.167 K s^{-1} for the temperature range between (273.15 and 373.15) K.

Viscosity and density measurements. Measurements of viscosity and density were performed using an automated SVM 3000 Anton Paar rotational Stabinger viscometer–densimeter. For the solid IL at room temperature, viscosities and densities were only determined above the respective melting temperature. The SVM 3000 Anton Paar rotational Stabinger viscometer–densimeter uses Peltier elements for fast and efficient thermostatization. Further details regarding the operation system can be found elsewhere.[14] The uncertainty in temperature is within ±0.02 K. The relative uncertainty in the dynamic viscosity is ±0.35% whereas the absolute uncertainty in density is $\pm 5 \times 10^{-4}$ g cm^{-3}. The measurements were carried out in the temperature range from (318.15 to 363.15) K for $[C_2C_1im][FAP]$, and from (338.15 to 363.15) K for $[C_2C_1im][PF_6]$, and at $\approx$0.1 MPa.

Mutual solubilities measurements. The mutual solubility measurements between water and ILs were carried out at temperatures from (288.15 to 363.15) K and at atmospheric pressure. The IL and the water phases were initially vigorously agitated and allowed to reach saturation equilibrium, and the complete phase separation, for at least 48 h for the mixtures involving $[C_2C_1im][FAP]$, in the whole temperature range, and for $[C_2C_1im][PF_6]$ at temperatures below 333.15 K. This period proved to be the minimum time required to guarantee a complete separation of the two phases and that no further variations in mole fraction solubilities occurred. Due to the high melting temperatures of $[C_2C_1im][PF_6]$, the solubility of water in this IL was only measured in their liquid state—in the temperature range from (333.15 to 363.15) K. Prior to our work, Wong *et al.*[10] have observed the formation of white solid flakes, indicative of the IL anion degradation, when the mixture was placed at high temperatures for more than 48 h. For that reason, in this work, the liquid–liquid phase behaviour of the binary system $[C_2C_1im][PF_6]$ + H_2O at temperatures above 333.15 K was determined after 2 h of equilibration. This period of time proved to be enough for the two liquid phases to remain stable and clear throughout the measurement period and from (333.15 to 363.15) K. The temperature was maintained by keeping the glass vials containing the phases in equilibrium inside an aluminium block specially designed for the purpose, which is further placed in an isolated air bath capable of maintaining the temperature within ±0.01 K. The temperature control was achieved using a PID temperature controller driven by a calibrated Pt100 (class 1/10) temperature sensor inserted in the aluminium block. In order to reach temperatures below room temperature, a thermostatized bath was coupled to the overall oven system. The solubility of water in the IL-rich phase was determined using a Metrohm 831 Karl–Fischer (KF) coulometer and the solubility of ILs in the water-rich phase was determined by UV-spectroscopy, using a SHIMADZU UV-1700 Pharma-Spec Spectrometer, at a wavelength of 211 nm, and using calibration curves previously established. Both phases were sampled at each temperature from the equilibrium vials using glass syringes maintained dry and at the same temperature of the measurements. For the IL-rich phase, samples of $\approx$0.1 g were taken and directly injected in the KF coulometric titrator. For the water-rich phase, and according to the detection limits of the equipment, the dilution factor for $[C_2C_1im][FAP]$ was *circa* 1 : 50 (w/w) times, while for $[C_2C_1im][PF_6]$ it was around 1 : 5000 (w/w) (substantially higher solubility in water). The mutual solubility results are an average of at least five independent measurements carried out at each temperature.

Molecular dynamics simulations

Condensed-phase Molecular Dynamics (MD) simulations of the $[C_2C_1im][FAP]$ and $[C_2C_1im][PF_6]$ pure ILs and their aqueous mixtures were carried out using the DLPOLY package.[34] Water and all ILs were modelled using the SPC model[35] and a previously described all atom force field (CL&P),[22,23,29] respectively. The latter is based on the OPLS-AA framework[36] but was to a large extent developed specifically to encompass entire IL families.

For the pure ILs, we started from low-density configurations composed of 200 ion pairs. For the mixtures, we also started from low-density initial configurations composed either of 1 ion pair and 600 water molecules (water-rich mixtures) or 200 IL ion pairs and 20 water molecules (IL-rich mixtures). For $[C_2C_1im][PF_6]$ we also performed simulations with 11 water molecules and 200 ion pairs in order to compare ($[C_2C_1im][FAP]$ + water and $[C_2C_1im][PF_6]$ + water) mixtures where the water molecules occupy approximately the same volume fraction.

The boxes were equilibrated under isothermal–isobaric ensemble conditions for 1 ns at 338 K and 1 atm using the Nosé–Hoover thermostats and isotropic barostats with time constants of 0.5 and 2 ps, respectively. Electrostatic interactions were treated using the Ewald summation method considering six reciprocal-space vectors, and repulsive-dispersive interactions were explicitly calculated below a cut-off distance of 1.6 nm (long-range corrections were applied assuming the system has an uniform density beyond that cut-off radius). Details concerning this type of simulation can be found elsewhere.[22,23,29] Several consecutive simulation runs of 1 ns were used to produce equilibrated systems—at least four runs in the case of water-rich mixtures and at least eight runs in the case of IL-rich mixtures or neat ILs—and to obtain the trajectories used to acquire the pertinent structural data.

Conclusions

In this work, the mutual solubilities with water, and the density and viscosity of pure $[C_2C_1im][PF_6]$ and $[C_2C_1im][FAP]$, were experimentally determined. Both ILs were chosen to address the effect of the fluorinated alkyl chains in the anion through their thermophysical properties and aqueous phase behaviour. Nevertheless, it should be remarked that further investigations with other fluorinated ionic liquids are still required to fully address this effect.

The mutual solubility results reveal that $[PF_6]$-based ILs are more soluble with water when compared to [FAP]-based compounds combined with a similar cation. The experimental densities of $[C_2C_1im][FAP]$ are higher than that for $[C_2C_1im][PF_6]$, while experimental viscosities follow an opposite trend.

The solubility results could be rationalized using MD simulation data that highlighted the difference between the two ILs in terms of their structure—and resulting differences in molar volume—and their interactions with the water molecules, namely the loss of crucial anion–water interaction centres when three of the fluorine atoms of the $[PF_6]^-$ anion are replaced by three perfluoroethyl groups in $[FAP]^-$.

Acknowledgements

This work was financed by national funding from FCT-*Fundação para a Ciência e a Tecnologia*, through the projects PTDC/AAC-AMB/119172/2010, FCT-ANR/CTM-NAN/0135/2012 (including a post-doctoral grant of K. Shimizu), PTDC/CTM-NAN/121274/2010, PEst-OE/QUI/UI0100/2013 and PEst-C/CTM/LA0011/2013. C.M.S.S. Neves and K.A. Kurnia also acknowledge FCT for their doctoral (SFRH/BD/70641/2010) and post-doctoral (SFRH/BPD/41781/2007) grants. M. G. Freire acknowledges the European Research Council (ERC) for the Starting Grant ERC-2013-StG-337753.

Notes and references

1 R. D. Rogers and K. R. Seddon, *Science*, 2003, **302**, 792–793.
2 M. J. Earle, J. M. S. S. Esperança, M. A. Gilea, J. N. Canongia Lopes, L. P. N. Rebelo, J. W. Magee, K. R. Seddon and J. A. Widegren, *Nature*, 2006, **439**, 831–834.
3 N. V. Plechkova and K. R. Seddon, *Chem. Soc. Rev.*, 2008, **37**, 123–150.
4 T. M. Letcher, D. Ramjugernath, K. Tumba, M. Królikowski and U. Domańska, *Fluid Phase Equilib.*, 2010, **294**, 89–97.
5 C. M. S. S. Neves, A. R. Rodrigues, K. A. Kurnia, J. M. S. S. Esperança, M. G. Freire and J. A. P. Coutinho, *Fluid Phase Equilib.*, 2013, **358**, 50–55.
6 U. Domańska, M. Królikowski, A. Pobudkowska and P. Bocheńska, *J. Chem. Thermodyn.*, 2012, **55**, 225–233.
7 U. Domańska and A. Marciniak, *Green Chem.*, 2007, **9**, 262–266.
8 N. Papaiconomou, N. Yakelis, J. Salminen, R. Bergman and J. M. Prausnitz, *J. Chem. Eng. Data*, 2006, **51**, 1389–1393.
9 V. Najdanovic-Visak, J. M. S. S. Esperança, L. P. N. Rebelo, M. N. da Ponte, H. J. R. Guedes, K. R. Seddon and J. Szydlowski, *Phys. Chem. Chem. Phys.*, 2002, **4**, 1701–1703.
10 D. S. H. Wong, J. P. Chen, J. M. Chang and C. H. Chou, *Fluid Phase Equilib.*, 2002, **194–197**, 1089–1095.
11 L. P. N. Rebelo, V. Najdanovic-Visak, Z. P. Visak, M. Nunes da Ponte, J. Szydlowski, C. A. Cerdeiriisña, J. Troncoso, L. Romaní, J. M. S. S. Esperança, H. J. R. Guedes and H. C. de Sousa, *Green Chem.*, 2004, **6**, 369.
12 C. M. S. S. Neves, M. L. S. Batista, A. F. M. Cláudio, L. M. N. B F. Santos, I. M. Marrucho, M. G. Freire and J. A. P. Coutinho, *J. Chem. Eng. Data*, 2010, **55**, 5065–5073.
13 M. G. Freire, C. M. S. S. Neves, K. Shimizu, C. E. S. Bernardes, I. M. Marrucho, J. A. P. Coutinho, J. N. Canongia Lopes and L. P. N. Rebelo, *J. Phys. Chem. B*, 2010, **114**, 15925–15934.
14 P. J. Carvalho, T. Regueira, L. M. N. B. F. Santos, J. Fernandez and J. A. P. Coutinho, *J. Chem. Eng. Data*, 2010, **55**, 645–652.

15 C. M. S. S. Neves, P. J. Carvalho, M. G. Freire and J. A. P. Coutinho, *J. Chem. Thermodyn.*, 2011, **43**, 948–957.
16 N. V. Ignat'ev, U. Welz-Biermann, A. Kucheryna, G. Bissky and H. Willner, *J. Fluorine Chem.*, 2005, **126**, 1150–1159.
17 D. Almantariotis, S. Stevanovic, O. Fandiño, A. S. Pensado, A. A. H. Pádua, J.-Y. Coxam and M. F. Costa Gomes, *J. Phys. Chem. B*, 2012, **116**, 7728–7738.
18 Q.-S. Liu, J. Tong, Z.-C. Tan, U. Welz-Biermann and J.-Z. Yang, *J. Chem. Eng. Data*, 2010, **55**, 2586–2589.
19 S. Seki, N. Serizawa, K. Hayamizu, S. Tsuzuki, Y. Umebayashi, K. Takei and H. Miyashiro, *J. Electrochem. Soc.*, 2012, **159**, A967–A971.
20 M. Součková, J. Klomfar and J. Pátek, *J. Chem. Thermodyn.*, 2012, **48**, 267–275.
21 NIST Chemistry Webbook at http://webbook.nist.gov/chemistry/.
22 J. N. Canongia Lopes and A. A. H. Pádua, *J. Phys. Chem. B*, 2004, **108**, 16893–16898.
23 K. Shimizu, D. Almantariotis, M. F. Costa Gomes, A. A. H. Pádua and J. N. Canongia Lopes, *J. Phys. Chem. B*, 2010, **114**, 3592–3600.
24 M. G. Freire, C. M. S. S. Neves, P. J. Carvalho, R. L. Gardas, A. M. Fernandes, I. M. Marrucho, L. M. N. B. F. Santos and J. A. P. Coutinho, *J. Phys. Chem. B*, 2007, **111**, 13082–13089.
25 M. G. Freire, P. J. Carvalho, R. L. Gardas, I. M. Marrucho, L. M. N. B. F. Santos and J. A. P. Coutinho, *J. Phys. Chem. B*, 2008, **112**, 1604–1610.
26 S. Martinho, J. M. M. Araújo, L. P. N. Rebelo, A. B. Pereiro and I. M. Marrucho, *J. Chem. Thermodyn.*, 2013, **64**, 71–79.
27 M. A. A. Rocha, C. F. R. A. C. Lima, L. R. Gomes, B. Schröder, J. A. P. Coutinho, I. M. Marrucho, J. M. S. S. Esperança, L. P. N. Rebelo, K. Shimizu, J. N. Canongia Lopes and L. M. N. B. F. Santos, *J. Phys. Chem. B*, 2011, **115**, 10919–10926.
28 A. B. Pereiro, M. J. Pastoriza-Gallego, K. Shimizu, I. M. Marrucho, J. N. Canongia Lopes, M. M. Piñeiro and L. P. N. Rebelo, *J. Phys. Chem. B*, 2013, **117**, 10826–10833.
29 J. N. Canongia Lopes, J. Deschamps and A. A. H. Pádua, *J. Phys. Chem. B*, 2004, **108**, 2038–2047.
30 O. Borodin, *J. Phys. Chem. B*, 2009, **113**, 12353–12357.
31 U. L. Bernard, E. I. Izgorodina and D. R. MacFarlane, *J. Phys. Chem. C*, 2010, **114**, 20472–20478.
32 F. S. Oliveira, A. B. Pereiro, J. M. M. Araújo, C. E. S. Bernardes, J. N. Canongia Lopes, S. Todorovic, G. Feio, P. L. Almeida, L. P. N. Rebelo and I. M. Marrucho, *Phys. Chem. Chem. Phys.*, 2013, **15**, 18138–18147.
33 K. Ueno, H. Tokuda and M. Watanabe, *Phys. Chem. Chem. Phys.*, 2010, **12**, 1649–1658.
34 W. Smith and T. R. Forester, *The DL_POLY Package of Molecular Simulation Routines (v.2.2)*, 2006.
35 M. Praprotnik, D. Janežič and J. Mavri, *J. Phys. Chem. A*, 2004, **108**, 11056–11062.
36 W. L. Jorgensen, D. S. Maxwell and J. Tirado-Rives, *J. Am. Chem. Soc.*, 1996, **118**, 11225–11236.

